HHS Public Access

Author manuscript

Med Phys. Author manuscript; available in PMC 2018 December 01.

Published in final edited form as:

Med Phys. 2017 December ; 44(12): 6589–6602. doi:10.1002/mp.12592.

Calibration and Error Analysis of Metal-Oxide-Semiconductor Field-Effect Transistor Dosimeters for Computed Tomography Radiation Dosimetry

Sigal Trattner, PhD[1], **Peter Prinsen, PhD**[2], **Jens Wiegert, PhD**[2], **Elazar-Lars Gerland, PhD**[3], **Efrat Shefer, PhD**[3], **Tom Morton, PhD**[4], **Carla M. Thompson, PhD**[5], **Yoad Yagil, PhD**[3], **Bin Cheng, PhD**[6], **Sachin Jambawalikar, PhD**[7], **Rani Al-Senan**[7], **Maxwell Amurao, PhD**[7], **Sandra S. Halliburton, PhD**[4,5], and **Andrew J. Einstein, MD, PhD**[1,7]

[1]Department of Medicine, Division of Cardiology, Columbia University Medical Center and New York-Presbyterian Hospital, New York, NY 10032, USA [2]Philips Research, Eindhoven, 5656AE, The Netherlands [3]Philips Healthcare, Haifa, 31004, Israel [4]Philips Healthcare, Cleveland, OH, 44143, USA [5]Imaging Institute, Division of Radiology, Cleveland Clinic, Cleveland, OH, Lerner Research Institute, Department of Biomedical Engineering, Cleveland Clinic, Cleveland, OH, 44195, USA and Department of Chemical and Biomedical Engineering, Cleveland State University, Cleveland, OH, 44195, USA [6]Department of Biostatistics, Columbia University Mailman School of Public Health, New York, NY, 10032, USA [7]Department of Radiology, Columbia University Medical Center and New York-Presbyterian Hospital, New York, NY 10032, USA

Abstract

Purpose—Metal-oxide-semiconductor field-effect transistors (MOSFETs) serve as a helpful tool for organ radiation dosimetry, and their use has grown in computed tomography (CT). While different approaches have been used for MOSFET calibration, those using the commonly-available 100 mm pencil ionization chamber have not incorporated measurements performed throughout its length, and moreover no previous work has rigorously evaluated the multiple sources of error involved in MOSFET calibration. In this paper we propose a new MOSFET calibration approach to translate MOSFET voltage measurements into absorbed dose from CT, based on serial measurements performed throughout the length of a 100 mm ionization chamber, and perform an analysis of the errors of MOSFET voltage measurements and four sources of error in calibration.

Methods—MOSFET calibration was performed at two sites, to determine single calibration factors for tube potentials of 80, 100, and 120 kVp, using a 100 mm long pencil ion chamber and a cylindrical computed tomography dose index (CTDI) phantom of 32 cm diameter. The dose profile along the 100 mm ion chamber axis was sampled in 5 mm intervals by nine MOSFETs in the nine holes of the CTDI phantom. Variance of the absorbed dose was modeled as a sum of the MOSFET voltage measurement variance and the calibration factor variance, the latter being comprised of three main subcomponents: ionization chamber reading variance, MOSFET-to-

Corresponding author: Andrew J. Einstein, MD, PhD, andrew.einstein@columbia.edu, Work Tel: 212-305-4275, Fax no: 212-305-4648, Postal Address: 622 West 168th Street, PH 10-203A, New York, NY 10032, USA.

MOSFET variation and a contribution related to the fact that the average calibration factor of a few MOSFETs was used as an estimate for the average value of all MOSFETs. MOSFET voltage measurement error was estimated based on sets of repeated measurements. The calibration factor overall voltage measurement error was calculated from the above analysis.

Results—Calibration factors determined were close to those reported in the literature and by the manufacturer (~ 3mV/mGy), ranging from 2.87 to 3.13 mV/mGy. The error σ_V of a MOSFET voltage measurement was shown to be proportional to the square root of the voltage V: $\sigma_V = \sqrt{cV}$ where $c = 0.11$ mV. A main contributor to the error in the calibration factor was the ionization chamber reading error with 5% error. The usage of a single calibration factor for all MOSFETs introduced an additional error of about 5-7%, depending on the number of MOSFETs that were used to determine the single calibration factor. The expected overall error in a high dose region (~30 mGy) was estimated to be about 8%, compared to 6% when an individual MOSFET calibration was performed. For a low-dose region (~3 mGy) these values were 13% and 12%.

Conclusions—A MOSFET calibration method was developed using a 100 mm pencil ion chamber and a CTDI phantom, accompanied by an absorbed dose error analysis reflecting multiple sources of measurement error. When using a single calibration factor, per tube potential, for different MOSFETs, only a small error was introduced into absorbed dose determinations, thus supporting the use of such a calibration factor for experiments involving many MOSFETs, such as those required to accurately estimate radiation effective dose.

Keywords

MOSFET; ion chamber; dosimetry; calibration; measurement error

1 Introduction

Radiation dosimetry in computed tomography (CT) is aimed at evaluating the amount of radiation received from CT scans and ensuring patient safety. Measuring organ dose using metal- oxide-semiconductor field-effect transistor (MOSFET) detectors has been validated [1-3] to be a useful approach for assessing radiation doses and has gained popularity over recent years. MOSFETs provide immediate read-out dose determinations and are simple to operate. A common use of MOSFETs is in anthropomorphic phantoms, where MOSFETs are positioned in organs of interest for dosimetry, in different locations within the phantom.

MOSFET measurements represent a change in voltage, proportional to the absorbed dose, and require careful calibration to relate the voltage to dose. Due to MOSFET energy dependence of about 10% in the 40–120 kVp range[4], calibration has to be performed for each tube voltage of interest. Ionization chambers (“ion chambers”) are considered to be the “gold standard” [5, 6] for radiation dose measurements due to their precision and linearity of response. Various MOSFET calibration methods, which use ion chambers, are reported in the literature. The calibration procedures are executed “in air”[4,7-9] or in phantoms, with different ion chamber models and using CT scanners or radiographic X-ray tubes[4,10-12]. While a calibration factor is based on the ratio between MOSFET voltage measurements and an ion chamber dose reading, calibration methods use different approaches to compare the

ion chamber readings and the MOSFETs' voltage measurements. The ion chamber reading reflects a certain irradiated region, not necessarily identical to, and indeed usually longer than, the region that the MOSFET measures; different approaches use different sampling numbers of MOSFET measurements for comparison with the ion chamber reading.

A 100 mm pencil ion chamber is commonly used for computed tomography dose index (CTDI) measurements and has been used for calibrating MOSFETs as well.[11, 12] While the ion chamber reading represents an average dose along its 100 mm length [13], typically only a few MOSFET readings are taken into consideration for the purpose of calibration.[11, 12]

This paper introduces a MOSFET calibration method motivated by the need to obtain a calibration factor for MOSFET measurements in anthropomorphic phantom CT dosimetry. The method presented uses a pencil ion chamber of 100 mm length and 21 MOSFET sample readings performed at 5 mm intervals spaced throughout the 100 mm length. It is performed in each of the nine holes in the standard CTDI phantom, constituting the center hole as well as four holes at the periphery of the head and body modules. An error analysis is performed to model the multiple potential sources of error of the determined dose, as detailed in section 2.4, which is comprised of a MOSFET voltage measurement error as well as errors from the calibration factor that is introduced by the calibration method suggested herein.

2 Materials and methods

2.1 Study overview

In this paper we describe a calibration method using a pencil ion chamber that determines the tube voltage (V_t)-dependent calibration factor, CF_{V_t}, relating the MOSFET voltage measurement V to a radiation dose D:

$$D = \frac{V}{CF_{V_t}}. \quad (1)$$

Section 2.2 describes the scanners, scan settings and sites used, as well as the different dosimetry equipment that is used for the calibration measurements. Section 2.3 describes how the calibration measurements are performed and how the calibration factor is calculated from these measurements. Section 2.4 describes the error $\sigma_{\text{tot}}(D)$ associated with determination of absorbed dose. This error has two sources: (1) the MOSFET voltage measurement error, $\sigma(V)$, which is voltage dependent as shown in section 2.4.1, and (2) the calibration factor error, $\sigma(\text{CF}_{V_t})$, which results from the calibration process and is modeled by four subcomponents that contribute to the error as detailed in section 2.4.2. For comparison with the calibration method proposed using a 100 cm pencil ionization chamber, we also perform MOSFET calibration experiments using a Farmer®-type small volume ion chamber, as described in section 2.5.

2.2 Calibration Measurements

Calibration measurements were performed on two 256-slice scanners (Brilliance iCT, Philips) at different sites (site 1: Philips Healthcare, Cleveland, OH, and site 2: Cleveland clinic, OH). Axial scans were performed with a collimation of 16×0.625 mm (10 mm), at tube voltages of 80, 100, and 120 kVp, with tube current-time products of 690, 400, and 240 mAs, respectively, and measured HVLs of 6.4 ± 0.4 mm Al, 7.7 ± 0.4 mm Al, and 8.8 ± 0.4 mm Al. The relatively narrow collimation was chosen to achieve a dose distribution along the 100 mm length of the ion chamber with both a region of direct (in-field) radiation and a significant region with only indirect (i.e. scattered) radiation; an example of such a dose distribution is illustrated in Figure 1. Thus, dosimetry measurements and hence the derived calibration factor include contributions from both direct and indirect irradiation. Maximal dose was controlled by scan parameter values to make sure that the dose in the tails of the dose profile was not too low, to minimize reading errors. MOSFETs were positioned in the nine holes of the CTDI phantom and their readings were compared with similarly positioned ion chamber readings.

CTDI phantom—A standard 32 cm diameter cylinder polymethyl methacrylate (PMMA) CTDI phantom of 14 cm depth (West Physics Consulting, Atlanta, GA) was used. The CTDI phantom has nine removable acrylic inserts of 1 cm diameter in nine holes, as shown in Figure 2: one at the center, four at the periphery (at clock positions 3:00, 6:00, 9:00, and 12:00) and four at the midway part, between the periphery and the center (at clock positions 1:30, 4:30, 7:30 and 10:30). In these holes the measuring devices, i.e. the ion chamber and the MOSFETs in custom-made holders, were inserted, as shown in Figure 3.

Ion chamber—A 100 mm long pencil ion chamber with air-equivalent walls (10X6-3CT; Accu-Dose 2186; Radcal, Monrovia, California) [15] was used, including a control unit that provides automatic correction for temperature, pressure and chamber calibration. A reading of this ion chamber represents the average exposure (or air kerma) over the chamber length l of 100 mm.

Calibrations were performed with a single axial rotation around the ion chamber long (z−) axis with stationary CT scanner bed[13]. An example for dose profile $D(z)$ is shown in Figure 1. The reading of the ion chamber in air kerma units, I, is related to the dose profile $D(z)$ by:

$$I=\frac{1}{fl}\int_{-l/2}^{l/2}D(z)dz, \quad (2)$$

where f is the f-factor converting air kerma to dose in air: f=1 mGy/mGy[13] in the energy-range relevant for CT and l is the chamber length as above.

MOSFETs—Two readers of a mobileMOSFET dose verification system were used (TN-RD-70W; Best Medical, Ottawa, Canada) in combination with high-sensitivity MOSFETs (TN-1002RD-H; Best Medical, Ottawa, Canada). Each reader can be attached to up to 5

MOSFETs. A Bluetooth wireless device communicated voltage data from the MOSFET readers to a PC laptop with MOSFET software installed.

Custom-made holders were used for inserting the MOSFETs in the CTDI phantom. The holders were made of PMMA, 14 cm length, each with a groove at its center that can contain a single MOSFET. Each holder was marked with lines at 5 mm intervals as can be seen in Figure 3.

Each MOSFET was used until its cumulative voltage reached 5000 mV because of potential changes in sensitivity beyond this value; this dose level was never reached during a calibration process, thus, MOSFETs were not replaced while calibrating.

2.3 MOSFET Calibration

The center of the CTDI phantom was placed at the isocenter of the CT scanner with the axes of its holes along the z-direction of the scanner. A dose measurement was performed in each of the nine holes using the ion chamber. The x-ray beam was collimated such that its profile in the z-direction was symmetric around the isocenter of the scanner and the ion chamber was positioned with its center aligned with the center of the hole. Eight consecutive measurements of single axial acquisitions were performed with a fixed delay between each scan, after which a reading was taken. The delay was chosen such that it resulted in eight different tube start positions distributed uniformly over the 360 degrees of a full rotation. This procedure was performed for each of the holes.

Nine MOSFETs in their respective holders (one MOSFET per holder) were then inserted into the nine holes and positioned such that each of them was exactly in the middle of the hole. They were then shifted in 5 mm steps, using the lines on the holders, along the z-direction for a total of 10 steps (see Figure 4) to the + z-direction of the initial center position, and 10 steps to the - z-direction of the center position. At each set of holder positions (center, left of center, and right of center) eight axial scans were performed, similar to the scan procedure of the ion chamber, irradiating all nine MOSFETs simultaneously. Thus, measurements were performed at a total of 21 measurement points at 5mm sampling intervals, thereby covering the 100 mm measuring range of the ion chamber, for each of the nine holes.

With a beam width of 10 mm, the dose at the edges of the dose distribution was on average 6% of the dose at the peak of the dose distributions for the periphery holes, 19% for midway holes and 28% for the center hole, at both sites.

The calibration was performed for tube voltages of 80, 100 and 120 kVp and calibration factors were calculated for each tube voltage separately.

During calibration MOSFET dosimeters were placed with their “bubble side” facing up. Our calibration method includes measurements throughout the 100 mm dose distribution, in nine different depths, thus, multiple angles of photons incident on MOSFETs are met in and off of isocenter during calibration and are taken into account within the final calibration factor. Moreover, MOSFETs are irradiated from a range of directions, both during the calibration and during the measurements, due to the rotation of the CT tube in a scan. Therefore,

MOSFET angular dependence (reported as 2% by the manufacturer) is not considered to have a significant effect on our measurement results.

For comparison with the ion chamber measurements, an average MOSFET value was calculated by integrating the voltage under the curve (similar to the dose distribution curve of Figure 1) and dividing by 100 mm. We approximated the integration by the trapezoidal rule leading to the following expression for the calibration factor CF_{h,V_t} of hole h, h=1…H, where $H=9$ in our calibrations, and tube voltage V_t, V_t =80, 100, 120 kVp:

$$CF_{h,V_t}=\frac{\sum_{k=2}^{20}V_k\Delta x+\sum_{k=1,21}\frac{V_k\Delta x}{2}}{lI_{\mathrm{avg},h}}, \quad (3)$$

where V_k is the average MOSFET reading (total reading divided by 8 measurements) for position k (corresponding to the lines on the holder), Δx=5 mm, l=100 mm and $I_{avg,h}$ is the average ion chamber reading (total reading divided by 8) per hole. As the final calibration factor CF_{V_t} we used the average of the values of the $H=9$ holes:

$$CF_{V_t}=\frac{1}{\mathrm{H}}\sum_{h=1}^{\mathrm{H}}CF_{h,V_t}. \quad (4)$$

This calibration factor translates the voltage into dose in air (due to the fact that the ion chamber reports dose in air, regardless of the phantom in which calibration took place), which later can be converted into dose in the relevant tissue or organ based on the MOSFET location in the phantom.

The error introduced by this type of calibration is discussed in the next section.

2.4 Absorbed dose error estimation

The absorbed dose error, $\sigma_{\mathrm{tot}}(D)$, can be split approximately into an error due to the MOSFET voltage measurement and an error due to the MOSFET calibration:

$$\sigma^2_{\text{tot}}(D)=\frac{1}{[E(CF_{V_t})]^2}\sigma^2(V) +[E(V)]^2\sigma^2\left(\frac{1}{CF_{V_t}}\right) +\sigma^2(V)\sigma^2\left(\frac{1}{CF_{V_t}}\right)\approx\frac{1}{[E(CF_{V_t})]^2}\sigma^2(V) +[E(V)]^2\sigma^2\left(\frac{1}{CF_{V_t}}\right)\approx\frac{1}{[E(CF_{V_t})]^2}\sigma^2(V) +\frac{[E(V)]^2}{[E(CF_{V_t})]^4}\sigma^2(CF_{V_t}). \quad (5)$$

Here $\sigma^2()$ denotes variance and $E()$ denotes expected value or mean. The first equality follows from Eq. (1) and the independence of CF and V. The voltage measurement error $\sigma(V)$ is mainly a random one, while the calibration error $\sigma(CF_{V_t})$ is mainly systematic, as shown in the following sections.

2.4.1 MOSFET voltage measurement error $\sigma(V)$—One of the potential contributions to the first term in Eq. 5, the MOSFET voltage measurement error, $\sigma(V)$, originates from the fact that the voltage is measured in a relatively small volume of the MOSFET (the active region is about 0.2 mm × 0.2 mm × 1 μm[22]), potentially making fluctuations in the number of X-ray quanta interacting in the volume relevant.

The MOSFET voltage V is proportional to the deposited dose, and since the deposited dose is proportional to the total energy, U_{tot}, deposited in the MOSFET by the N interacting photons, we conclude that

$$V\sim U_{\text{tot}}=\sum_{i=1}^{N}U_i,$$

where N obeys Poisson statistics and U_i are independent and identically distributed.

By virtue of the identity $\sigma^2(f(X,Y)) = E[\sigma^2(f(X|Y))] + \sigma^2(E[f(X|Y)])$ the variance of V is

$$\sigma^2(V)\sim\sigma^2(U_{\text{tot}})=E[N]\sigma^2(U)+(E[U])^2\sigma^2(N)\sim E[N],$$

where we used the Poisson statistics of the number of photons $\sigma^2(N)= E[N]$. Since $E[V]\sim E[N]$ we conclude that $\sigma^2(V)\sim E[V]$,. i.e. that the variance in the measured voltage is proportional to the mean measurement value:

$$\sigma^2(V)=cE[V], \quad (6)$$

where $E[V]$ is the expected value of the voltage V and c is a proportionality constant.

There are other errors contributing to the MOSFET measurement error but these are all much smaller than the error due to the fluctuations in the number of interacting quanta. Examples are the reader stability error, which is less than one percent of the maximum accumulated dose, ±1 mV, over one year[16], and the reader linearity error, which is less than 1% of the total dose reading, ±1 mV, over the full dose range[16]. We have not identified any other errors that are substantial enough to take into account in the error estimation.

We make a more accurate estimate of the value of c from measurements as follows. The contribution of each photon to the deposited energy (and thus to the MOSFET voltage) is proportional to its energy. The voltage distribution is thus a weighted sum of Poisson distributions[17]. Due to the complexity of this distribution, for practical reasons, we approximated it by a normal distribution. This approximation is justified by the fact that for large numbers of photons, according to the central limit theorem, the Poisson distribution can be approximated by a normal distribution and the weighted sum of normal distributions is again a normal distribution. We thus expect a single measurement of voltage V to follow the normal distribution $N(\mu, c\mu)$, where $\mu = E(V)$. The Maximum Likelihood Estimates (MLEs) of c and μ, $\tilde{c}$ and $\tilde{\mu}$, are then given by the following coupled equations:

$$\tilde{\mu}_j=\sqrt{\frac{1}{n}\sum_{i=1}^{n}V_{j,i}^2+\left(\frac{\tilde{c}}{2}\right)^2}-\frac{\tilde{c}}{2'}, \quad (7)$$

$$\tilde{c}=\frac{1}{N}\sum_{j=1}^{N}\frac{1}{n}\sum_{i=1}^{n}\frac{(V_{j,i}-\tilde{\mu})^2}{\tilde{\mu}_j}, \quad (8)$$

Here i is the index of a measurement in a set of n repeated measurements, j is the index of a measurement set, and $V_{j,i}$, $i = 1,\ldots, n$, $j = 1,\ldots, N$, follow $N(\mu_j, c\mu_j)$. We used data we had previously obtained from N=1006 MOSFET measurement sets that were each repeated n=5 times. A summary of the data that was used is given in Appendix A.

Using the asymptotic normal approximation, confidence intervals for the parameters were estimated. The 95% confidence intervals are $\tilde{\mu}_j(1 \pm 1.96\sqrt{\tilde{c}/5\tilde{\mu}_j})$ and $\tilde{c}(1 \pm 1.96\sqrt{2/5N})$. For $\tilde{\mu}_j$ this confidence interval should be regarded as a rough estimate considering the small number (five) of repeated measurements.

The variation between five measurements consists of a contribution from the random variation of the MOSFET measurements and of a contribution due to a different start angle

position of the tube in each scan. In order to remove the error due to the start angle variation, we performed Monte Carlo (MC) simulations for each measurement (taking into account the correct tube start angle) and then calculated a corrected MOSFET reading by multiplying the MOSFET reading with the average value of the MC results over the five measurements divided by the MC result for that particular measurement. The MC simulation is explained in more detail in Appendix B.

To examine whether our assumption about the distribution of measurement values is valid, we plotted the experimental cumulative distribution function (CDF) of $X_{j,i} \equiv (V_{j,i} - \tilde{\mu}_j)/\sqrt{\tilde{\mu}_j}$ for all $5N$ measurement points and compared it to the theoretical curve

$$\mathrm{CDF}(X;c) = \frac{1}{2}\left(1 + \mathrm{erf}\left[\frac{X}{\sqrt{2c}}\right]\right). \quad (9)$$

Here $\mathrm{erf}[x] = \frac{2}{\sqrt{\pi}}\int_0^x e^{-t^2}\,\mathrm{d}t$ is the error function.

2.4.2 Calibration factor error $\sigma(CF_{V_t})$—For the second term in Eq. 5, the calibration error, $\sigma(CF_{V_t})$, we have identified four main sources:

$$\sigma^2(CF_{V_t}) \approx \sigma^2_{\mathrm{VMOS}}(CF_{V_t}) + \sigma^2_{\mathrm{ion}}(CF_{V_t}) + \sigma^2_{\mathrm{MtoM}}(CF_{V_t}) + \sigma^2_{\mathrm{avg}}(CF_{V_t}). \quad (10)$$

The first contribution $\sigma^2_{\mathrm{VMOS}}(CF_{V_t})$ is due to the random error in the MOSFET voltage measurements for the calibration. This error is the same as discussed in the previous section, only now it applies to the MOSFET measurements for the calibration. $\sigma^2_{\mathrm{VMOS}}(CF_{V_t})$ can be determined by combining Eqs. (3), (4) and (6):

$$\sigma^2_{\mathrm{VMOS}}(CF_{V_t}) = \left(\frac{\Delta x}{Hl}\right)^2 \sum_{h=1}^{H}\left(\frac{1}{I_{\mathrm{avg},h}}\right)^2 \left(\sum_{k=2}^{20} cV_{k,h} + \frac{1}{4}\sum_{k=1,21} cV_{k,h}\right). \quad (11)$$

Although the voltage measurement error of each MOSFET is random, the use of a single calibration factor for different MOSFETs makes $\sigma_{\mathrm{VMOS}}(CF_{V_t})$ a systematic error.

The second error term, $\sigma_{\mathrm{ion}}(CF_{V_t})$, is the error of the ion chamber reading, which was provided by the manufacturer of the ion chamber.

The MOSFET-to-MOSFET variation of the calibration factor is, according to the manufacturer, related to small variations in the MOSFET encapsulation material thickness, which results in variation of attenuation in this material. This variation introduces an

additional error, $\sigma_{\mathrm{MtoM}}(CF_{V_t})$ when a single calibration factor is used for different MOSFETs. We determined the MOSFET-to-MOSFET variation from two different sets of measurements. The first one is of a set of 29 MOSFETs that were irradiated simultaneously with a uniform beam at 120 kVp and 70 mAs with Ti filter and bowtie filter removed. An MLE of $\tilde{V}_j$ for each set of 3 measurements lead to the same equation as Eq. (7) with $n = 3$ and $\tilde{c}$ replaced by the value determined as described in the previous section. From the variation of $\tilde{V}_j$ for j=1…29 we estimated the MOSFET-to-MOSFET variation.

The second set of measurements consisted of our calibration results. Since we determined a calibration factor in each of the nine holes of the CTDI phantom with a different MOSFET in each hole, we could use these measurements to determine the MOSFET-to-MOSFET variation.

The last error term, $\sigma_{\mathrm{avg}}(CF_{V_t})$, is related to this MOSFET-to-MOSFET variation. If N_{CM} calibration factors are determined, each with a different MOSFET, and the calibration factors are then averaged to obtain a single calibration factor, then this single calibration factor is only an estimate of the true average value. The error in this estimate is

$$\sigma_{\mathrm{avg}}(CF_{V_t}) = \frac{\sigma_{\mathrm{MtoM}}(CF_{V_t})}{\sqrt{N_{\mathrm{CM}}}}. \quad (12)$$

In our case, $N_{CM} = 9$.

2.5 Calibration experiments using a Farmer®-type small volume ion chamber

In the literature, alternative calibration methods have been suggested which employ a small volume ion chamber for MOSFET calibration, e.g. as in Brady and Kaufman's work on calibration in air and in a scattering medium[5]. Such calibration methods have been limited to in-field (i.e. within the x-ray beam) measurements. Our proposed calibration method in contrast uses a pencil ion chamber, which due to its longer z-axis coverage reflects not just in-field, but also out-of-field (beyond the x-ray beam) MOSFET positions, as well as different MOSFET depths within the CTDI phantom. While a disadvantage of our calibration approach is the larger number of measurements it requires, this longer z-axis coverage offers a potential advantage over calibration methods based on small volume ion chamber measurements. Specifically, in order to comprehensively characterize radiation doses throughout an anthropomorphic phantom from a particular scan protocol, MOSFETs used to determine organ doses need to be placed both at in-field and out-of-field locations. MOSFETs will also be in-field for part of the scan and out-of-field for the rest of the scan, e.g. in helical scans.

To compare our calibration method with a small volume ion chamber-based approach, and to understand the impact of different positions on the calibration factor, we performed additional MOSFET calibration experiments at both in-field and out-of-field locations using the commonly used Farmer ®-type small volume 0.6 cc ion chamber (model 10×5-0.6CT, Radcal, Monrovia, California), which has active length of about 2 cm. This Farmer chamber

was coupled with an ion chamber monitor (model 9095, Radcal, Monrovia, California) and placed in a CTDI phantom. Calibration here was performed on a GE LightSpeed VCT XTe (GE Healthcare, Waukesha, WI) 64-slice scanner using axial scans without table motion, with tube voltage 120 kVp, tube current 300 mA, 1 sec rotation time, 64×0.625 mm collimation and measured HVL of 7.7 mm Al. Beam width was chosen wide enough to ensure that the full length of the Farmer chamber (~23 mm) is in the beam. The Farmer chamber was placed in the middle of the x-ray beam, and equidistant in the z-axis from the edges of the CTDI phantom.

Calibration scans were performed with the Farmer chamber, placed in a PMMA holder, in several holes in the CTDI phantom—center hole, 12:00 hole, 3:00 hole, and 6:00 hole (see Figure 2) —to reflect different depths and positions relative to the scanner table. The MOSFET in its holder was also placed in each of these holes, in a position where the center of the Farmer chamber had been, and scanned. Each scan was performed three times in each position. Calibration factors for in-field positions were calculated by dividing averages of the MOSFET readings (mV) by average Farmer chamber readings (mGy), for each hole.

We also performed out-of-field calibration scans, outside of the x-ray beam, using the center hole, 12:00 hole, 3:00 hole, and 6:00 hole. First the Farmer chamber was placed approximately 2 cm past the edge of the x-ray beam and scanned. Then, the MOSFET was positioned sequentially in three positions: i) the Farmer chamber mid-position, i.e. where the center of the Farmer chamber was placed, ii) an additional 1 cm further past the edge of the x-ray beam in the z-axis, i.e. at the far end of the Farmer chamber, and iii) 1 cm closer to the edge of the x-ray beam in the z-axis, i.e. at the near end of the Farmer chamber. Thus these three positions span a total of 2 cm in the z-axis, which is the length of the Farmer chamber, and they are centered at the Farmer chamber mid-position. For out-of-field calibration, we determined calibration factors in two ways: i) by dividing the average MOSFET readings for which the MOSFET was in the Farmer chamber mid-position, by the average of the Farmer chamber readings, and ii) by dividing the average MOSFET readings for all three positions by the average of the Farmer chamber readings.

3 Results

3.1 MOSFET Calibration

Figure 5 shows the results of a calibration measurement at 120 kVp. MOSFET voltage measurements are plotted as a function of MOSFET location index $k = 1,\ldots 21$ for the nine different holes in the CTDI phantom (see Figure 2).

Table 1 reports the calibration factors, CF_{V_t}, calculated according to Eq. (3), for MOSFET calibrations that were performed at the two sites. Differences between calibration factors at the same tube voltages in the two sites were less than about 3%.

3.2 MOSFET voltage measurement error

Data points (tube start-angle corrected) were used from 1006 sets of five measurements (Appendix A). The resulting parameter value, calculated using Eqs. (7) and (8), was $c = 0.113\pm0.004$ mV (95% confidence interval). Measurements were split up according to tube

voltage and for each voltage a value of c was again determined. We found c = 0.102±0.015 mV (N = 67) at 80 kVp, c = 0.113±0.006 mV (N = 498) at 100 kVp, and c = 0.115±0.007 mV (N = 441) at 120 kVp.

Appendix C (see Figures C1 and C2) presents estimates of c in different MOSFET voltage regimes as well as a back-of-the-envelope order of magnitude estimation of c which shows that $c \approx 0.1$ mV for the particular MOSFETs that were used, thus, leading to an error of a few percent for typical MOSFET voltages, and showing this error is indeed significant.

Figure 6 displays the comparison between the CDF of all measurements (corrected for starting angle) and the theoretical curve (Eq. (9)) with c = 0.113 mV.

3.3 Calibration factor error

Using numbers from the calibration measurements with nine holes, H=9, and c = 0.113 in Eq. (11) leads to

$$\sigma^2_{\mathrm{VMOS}}(CF_{V_t}) = (0.01\mathrm{mv/mGy})^2. \quad (13)$$

The systematic error in the ionization chamber readings was 5%. The main contributions to this error were the calibration error of the ionization chamber (4%), the exposure rate dependence (2%) and the energy dependence (2%) [18]. The latter was actually reported as 5% in the specifications but a closer study of the ion chamber energy dependence graph showed that it was only 2% in the relevant energy range. We thus concluded that

$$\sigma^2_{\mathrm{ion}}(CF_{V_t}) \approx (0.05 CF_{V_t})^2. \quad (14)$$

This is more than an order of magnitude larger than $\sigma^2_{\mathrm{VMOS}}(CF_{V_t})$ for our MOSFETs.

The error due to the MOSFET-to-MOSFET variation, σ_{MtoM}, which was determined from two different sets of measurements, was expressed as a relative variation:

$$\sigma^2_{\mathrm{MtoM}}(CF_{V_t}) \approx (\alpha CF_{V_t})^2. \quad (15)$$

First we looked at 29 MOSFETs in a uniform field (120 kVp, 70 mAs, collimation 32×0.625 mm, no bow tie filter, titanium filter). We calculated the MLE estimate $\tilde{V}_j$ for each of the MOSFETs and then we estimated the mean $\hat{\mu}(\tilde{V}_j)$ = 31.2 mV and the variance $s^2(\tilde{V}_j)$ = 1.886 mV^2. The latter contains a contribution from the random error in a voltage measurement but due to the large number of MOSFETs this contribution could be neglected (it is ~$c\hat{\mu}(\tilde{V}_j)/(3 \times 29)$ = 0.01 mV^2). The estimate of the relative standard deviation for the MOSFET-to-MOSFET variation is therefore $\alpha = \sqrt{s^2(\tilde{V}_j)}/\hat{\mu}(\tilde{V}_j) = 0.044$ (the 95% confidence interval is

[0.033,0.055]). Figure 7 shows the distribution of the 29 values $X_j \equiv (\tilde{V}_j - \hat{\mu})/s$ and the standard normal distribution.

The second set of measurements that we used to determine the MOSFET-to-MOSFET variation consisted of the calculated calibration factors, per hole, in the CTDI phantom, and per tube voltage. The results of Site 1 are shown in Figure 8. The relative variation in calibration factor, with 95% confidence levels (in brackets), is α = 0.035 [0.018, 0.052] for 80 kVp, a = 0.037 [0.019, 0.055] for 100 kVp, and α = 0.062 [0.032, 0.091] for 120 kVp. For Site 2, we found relative variations of α = 0.052, α = 0.049 and α = 0.061 for 80 kVp, 100 kVp, and 120 kVp, respectively.

The last error term, $\sigma_{\text{avg}}(CF_{V_t})$, was derived from the MOSFET-to-MOSFET variation values that were presented above, per tube voltage, divided by the square root of N_{CM} = 9 holes of the CTDI phantom that had been used, as seen in Equation (12).

3.4 Absorbed dose error

We showed that $\sigma^2_{\text{VMOS}}(CF_{V_t})$ is negligible when nine (or down to five) holes are used, compared to at least one of the remaining errors; see Eqs. (13) and (14). Of the remaining errors, $\sigma^2_{\text{ion}}(CF_{V_t})$ and $\sigma^2_{\text{MtoM}}(CF_{V_t})$ were comparable in size, see Eqs. (14) and (15), respectively, while $\sigma^2_{\text{avg}}(CF_{V_t})$ was comparable or smaller, see Eq. (12). For obtaining $\sigma^2_{\text{MtoM}}(CF_{V_t})$ we determined a in two different ways and for three different tube voltages. Although there was some variation in the results, deviations from the average value a = 0.05 were small and this value of a was inside the 95% confidence interval for all results. In summary, the relative variance in absorbed dose determination, using the value a = 0.05, c = 0.11, is

$$\frac{\sigma^2_{\text{tot}}(D)}{D^2} \approx \frac{0.11\text{mV}}{V} + 0.05^2 \left(2 + \frac{1}{N_{\text{CM}}}\right). \quad (16)$$

To illustrate the effect of using a single calibration factor for all MOSFETs vs calibrating every MOSFET individually we calculated the difference in total error. Taking a = 0.05, a single calibration factor for all MOSFETs introduced an additional error of $0.05\sqrt{1+1/N_{\text{CM}}} = 5-7\%$ (depending on the number of MOSFETs/holes, N_{CM} that were used in the calibration process). Its contribution to the total error was smaller though, due the presence of other errors (and the way variances are combined to determine the total error): if we consider a typical absorbed dose value in the direct beam of 30 mGy (approximate MOSFET measurement ~100 mV), the total error in the absorbed dose with individual calibration would be about 6% ($\sqrt{(0.11/100+0.05^2)}$), while with a single calibration factor it would be about 8% ($\sqrt{(0.11/100+0.05^2(2+1/9))}$. For a lower absorbed dose of 3 mGy (MOSFET measurement ~10 mV) these numbers would be 12% and 13% respectively.

3.5 Calibration using Farmer chamber

Conversion factors determined from the calibration experiments using the Farmer chamber are presented in Table 2. For in-field calibration a consistency in calibration factor values can be observed among the different holes, with an average of 2.89 mV/mGy and very low variation (coefficient of variation (CoV) 1.4%). In contrast, in out-of-field calibrations, we found greater variations among calibration factors in different holes (>5%), in both methods of calculation, using the MOSFET in the mid-position or in all three positions. The average calibration factor for in-field calibration, 2.89 mV/mGy was different than that for out-of-field positions, 3.09 (1 position) and 3.19 mV/mGy (3 positions), by 7% and 10%, respectively.

4 Discussion

Using the suggested calibration method in two scanners, of the same model/manufacturer at different sites with different MOSFETs, has shown consistency of the calculated calibration factors. The calibration factors for the different energies determined were in the range of 2.87 - 3.13 mV/mGy, close to the ~3 mV/mGy value reported in the literature [4,19-21].

Our calibration method included measurements at 21 positions, to characterize the dose distribution over a 100 mm length corresponding to the length of the pencil ion chamber. Several other publications which used the same pencil ion chamber have used five MOSFET samples[11, 12] and performed MOSFET measurements only at the center of radiation, in-field, in the center of the pencil ion chamber [11, 12]. Since the ion chamber reading represents the average exposure over the chamber length, more than five MOSFETs should be used, and not only in the center but along its full length, to sample the dose distribution correctly and achieve an appropriate comparison to the ion chamber reading.

The calibration method proposed in this study entails many scans, and yet this large amount of scans can be justified when a single calibration factor for different MOSFETs is used for experiments involving many measurements. The error due to the MOSFET-to-MOSFET variation could be avoided by calibrating each MOSFET individually. However, this is impractical in some cases; for example, we have performed CT dosimetry in anthropomorphic phantoms where we used a few hundred MOSFETs over several days. Calibrating each MOSFET would have been an onerous effort and costly due both to scanner time and also to the more frequent change of MOSFETs, which would have been required if each were calibrated individually, due to more quickly reaching the threshold accumulated voltage at which MOSFET noise increases and thus replacement is recommended. Moreover, the difference between the errors of a single calibration factor for different MOSFETs vs. those of an individual calibration factor for each MOSFET was very modest; we observed that the MOSFET total error for a single calibration factor vs. for an individual calibration factor was 8% vs 6% for a 100mV MOSFET measurement (~30 mGy) and 13% vs. 12% for a 10mV measurement.

The MOSFET calibration method suggested here was performed in a CTDI phantom, and not in air, since the purpose of calibration was to subsequently use the calibrated MOSFETs to perform in-phantom CT dosimetry. Thus, scattering is accounted for in the calibration

factor. According to Brady and Kaufman[4], who compared three methods of MOSFET calibration, in air and in a scattering medium, there is a need to calibrate in a scattering environment that is commensurate with the intended scattering environment of the MOSFETs, since the scatter has an effect on the calibration factor that may lead to dosimetry errors in the order of 12%. By using multiple positions, different scatter patterns are covered in the suggested method.

An important aspect that is taken into account in the method we present is the inclusion of different positions of the MOSFETs with respect to beam and different depths within the CTDI phantom, allowing for primary photons as well as scattered photons of various angles and, hence, various energies incident on the MOSFETs, to be reflected in the calibration process. Using different positions in the calibration process is compatible with experiments involving anthropomorphic phantom dosimetry where MOSFETs are placed in different positions within the anthropomorphic phantom. In different methods that were reported in the literature, where a scattering medium was used, calibration was performed in-field and in the center of the CTDI phantom (or other phantom) or near the surface (1 cm below) [4, 11, 12]. The latter might be an appropriate calibration in the case of MOSFET dosimetry close to the surface of the phantom.

In order to compare our calibration approach with an alternative approach using a small-volume ion chamber, we also performed calibration experiments using a Farmer chamber. It was shown for the Farmer chamber that calibration factors of a MOSFET in different in-field positions, were highly uniform (1.4% variation). However, when calibration procedures were performed out-of-field, at different depths, it resulted in larger (>5%) variation of calibration factors between different depths, and a 7-10% difference compared to the average calibration factor of in-field positions. These results point at an influence of the calibration position on the calibration factor, most likely due to different local primary spectra, the varying scatter patterns and the multiple angles of photon incidence on the MOSFETs. While the ideal calibration that is implicated is a per-position calibration, it is not a realistic solution. A virtue of our suggested method using the pencil ionization chamber is that it incorporates different scatter and angle patterns and reflects a range of in-field and out-of-field MOSFET positions at different depths.

Due to MOSFET energy dependence, MOSFET calibration factors were determined per tube voltage (kVp). Still, for a given kVp, variations of average photon energy between in-field and out-of-field regions occur, which might affect the calibration factor as we showed when using the Farmer ion chamber. For further understanding, we have run Monte Carlo simulations using Diagnostic Photon Simulations (DiPhoS, Philips Research, Eindhoven, Netherlands) on a voxelized CTDI phantom to evaluate local energy spectra. The simulations were performed using single rotation scans of the CTDI phantom with 2 cm collimation at 80, 100 and 120 kVps. The results show that there is a range of average energies both at in-field and at out-of-field locations, depending on the position of the MOSFET within each region. E.g., for 120 kVp scans, for which the average tube spectrum energy was 65 keV, for the in-beam region, the range of average energy was 59-64 keV, and for out-of-beam region it was a 51-53 keV (independent of distance from the direct beam). For the 80 kVp scans (average tube spectrum energy of 53 keV) for the in-beam region, the

range of average energy was 49-52 keV, and for the out-of-beam region it was a 44-46 keV. Thus, for a given tube voltage, MOSFET detectors are still exposed to different energy spectra. This will also be the case when MOSFETs are in-field for part of the scan and out-of-field for the rest of the scan, e.g. in helical scans. If we consider the 120 kVp case we see that the average energy in the out-of-beam region is slightly higher than the average in-beam energy for the 80 kVp case. The calibration factors for these kVp values differ by about 7% in our calibrations, giving some indication of the variation of the calibration factor that could be expected for a MOSFET at 120 kVp at different measurement locations. These are two extreme cases though: in our measurements both the calibration and the MOSFET measurements will be a combination of in-beam contributions and out-of-beam (scatter) contributions, so we expect the position dependent variation to be less than this, maybe a few percent. Even though this is possibly close to some of the other errors, it will not have a dramatic effect on the final error: in high dose regions the error is about 8%, as argued in section 3.4. If the error due to position dependence were 4%, this 8% would increase to 9%. The 13% error in the low dose regions would then increase by about 0.5%. Thus, the position dependence does potentially have an effect on the total error, albeit small. Still, further investigation is required to examine calibration factors tailored to each MOSFET position, for each type of scan, which would take into consideration the exact spectrum to which the MOSFET would be exposed.

The error of the absorbed dose determined using the MOSFETs was modeled as a sum of a random error in the MOSFET voltage measurement and a systematic error in the MOSFET calibration factor. The MOSFET voltage measurement error was modeled as voltage dependent, $\sigma^2(V) = cV$, where the voltage dependence of the error ($\sim\sqrt{V}$) was confirmed (Figure 6) as well as the normal approximation of its distribution. A constant value of c = 0.11 mV was found, neglecting a slight dependence of c on kVp and small effects owing to the MOSFET-to-MOSFET variation of c, which only had a small impact on the error. This value was very close to the theoretical estimate in Appendix C. Figures C1 and C2 in Appendix C demonstrated that there was no significant indication that c depends on the MOSFET voltage. Since the random error is proportional to the square root of the voltage, low voltages have relatively large errors while high voltages have relatively low errors. This agrees with the findings of Brady and Kaufman[4] and of Yoshizumi et al.[7]

Another potentially valid method for calibration, which was suggested in the context of CTDI, is described in the AAPM Report No.111[25]. A Farmer chamber is placed midway of a 45 cm-long PMMA phantom and the entire length is irradiated in a continuous (helical) or step-and-shoot (axial) mode. This approach ensures that > 98% of primary and scatter dose[26], even from a large scan length, is measured by the chamber and this result can then be compared with the reading of a MOSFET positioned and scanned similarly to the Farmer chamber.

Limitations of our findings are that we have not tested spectra that are qualitatively different from CT spectra, and that the value of c we determined here is only valid for the MOSFETs we used, with a sensitivity of about 3 mV/mGy. Additionally, one might argue that the start-angle correction we used in data points of voltage measurements, for eliminating the variation due to the tube start angle, also introduced variation due to errors in the MC

results. Although the MC simulations were performed with a sufficiently high number of photons so that statistical variations due to the finite number of photons are much smaller than the expected error in the measurements, there may be systematic errors due to the modeling of the scanner. Normally these would increase the variation so, if they were significant, they would lead to an overestimation of the value of c. Without the tube start angle correction $c = 0.165 \pm 0.006$ mV rather than 0.11 mV. This higher value can be considered an upper bound for the estimate of c. Finally, a sampling interval more granular than 5 mm can be used to better approximate the in-field radiation region.

5 Conclusions

For dose determination using MOSFETs in an anthropomorphic phantom, a calibration method for the MOSFETs was proposed for which the relative dose error is $\sqrt{\frac{0.11\text{mV}}{V}+0.05^2\left(2+\frac{1}{N_{\text{CM}}}\right)}$, for a single calibration factor. The use of a single calibration factor for an entire set of MOSFETs is practical when experimental dosimetry involves a large number of MOSFETs, and it was shown to have an error that is comparable to an individual calibration factor for each MOSFET.

The error in a MOSFET measurement consists of an error due to the voltage measurement and an error in the calibration factor. The former has one main component, which is proportional to the measured voltage. The main contributions to the calibration factor are the error due to the ion chamber and, in case MOSFETs are not calibrated individually, two errors due to the MOSFET-to-MOSFET variation. The first error is introduced because of the use of only a few MOSFETs to estimate the average calibration factor, and the second error is due to the use of this estimation of the average calibration factor instead of the actual calibration factor for each MOSFET.

The calibration method that is proposed incorporates both in-field and out-of field MOSFET measurements with MOSFETs located at several depths in a CTDI phantom. It thus samples a range of different energy spectra that a MOSFET might experience. Further investigation is encouraged to examine the location, orientation, and scan-type dependent variation of the calibration factor.

Acknowledgments

This work was supported by grant R01 HL109711 from the NHLBI and by an investigator-initiated research grant from Philips Healthcare.

Conflicts of Interest: Dr. Einstein has received research grants to Columbia University for other research from GE Healthcare and Toshiba America Medical Systems. Dr. Prinsen, Dr. Wiegert, Dr. Gerland, Dr. Shefer, Dr. Morton, Dr. Yagil and Dr. Halliburton are employees of Royal Philips.

6 Appendix

A. Overview of the data used for estimation of *c*

For estimation of c we used MOSFET voltage readouts previously recorded in dosimetry measurements using anthropomorphic phantom experiments. The data consists of readouts of MOSFETs that were placed in 46-50 different locations representing organs, in adult (male and female) and infant anthropomorphic phantoms (ATOM 701, ATOM 704-D, respectively; CIRS, Norfolk, VA). In total, we had N=1006 MOSFET measurement sets that were each repeated n=5 times.

Table A1 gives an overview of all scans performed on the anthropomorphic phantoms. For each scan the type of phantom (male, female, or infant) is indicated, as well as the region scanned (chest, abdomen, brain, cardiac, or chest-abdomen-pelvis), the scan mode (helical, prospective ECG-triggered axial (PTA), or retrospective ECG-gated helical (RGH)), and the peak tube potential (80, 100, or 120 kVp). $CTDI_{vol}$ per scan as well as scan length are also reported.

Table A1

Description of scans performed. Every scan series consists of five repeated scans.

Scan Series Number	Phantom	Scan Region	Scan Mode	Peak Tube Potential [kV]	$CTDI_{vol}$ per scan [mGy]	Scan Length [cm]
1	female	chest	helical	120	27.0	302.4
2	male	chest	helical	120	27.0	302.4
3	male	chest	helical	100	17.8	303.0
4	male	abdomen	helical	120	27.0	420.8
5	male	brain	helical	120	62.1	160.0
6	male	brain	helical	100	42.0	160.0
7	female	chest	helical	100	17.8	302.4
8	female	abdomen	helical	120	27.0	421.2
9	female	cardiac	PTA	120	29.5	140.4
10	female	cardiac	PTA	100	18.4	140.4
11	female	cardiac	PTA	80	8.2	140.4
12	female	cardiac	PTA	100	10.7	140.4
13	female	cardiac	RGH	120	51.3	140.4
14	female	cardiac	RGH	100	30.7	140.4
15	female	cardiac	RGH	120	51.3	140.4
16	male	cardiac	PTA	120	29.5	140.4
17	male	cardiac	PTA	100	18.4	140.4
18	male	cardiac	PTA	80	8.2	140.4
19	male	cardiac	PTA	100	10.7	140.4
20	male	cardiac	RGH	120	51.3	140.4

Scan Series Number	Phantom	Scan Region	Scan Mode	Peak Tube Potential [kV]	$CTDI_{vol}$ per scan [mGy]	Scan Length [cm]
21	male	cardiac	RGH	100	30.7	140.4
22	male	cardiac	RGH	120	51.3	140.4
23	infant	brain	helical	100	24.9	120.0
24	infant	chest	helical	100	17.6	180.0
25	infant	chest	helical	100	17.6	180.0
26	infant	chest-abdomen-pelvis	helical	100	9.3	315.0

PTA = prospective ECG-triggered axial, RGH = retrospective ECG-gated helical.

B. Correction of tube start angle in the data used for estimation of c

In order to correct the tube start angle we performed MC simulations using Diagnostic Photon Simulations (DiPhoS, Philips Research, Eindhoven, Netherlands).

In DiPhoS, photons were generated randomly with an energy distribution representative of X-rays after exiting the X-ray tube. These photons were transported through the tube housing and the phantom. The latter was located at the scanners isocenter, 57 cm from the focal spot. Interaction with a Ti filter (adult phantom) and the bowtie filter as well as collimation by the collimators were taken into account. The energy deposited in each voxel was tracked and was converted to dose by dividing by the mass of the voxel. Simulations were properly normalized by dividing by a kVp-dependent normalization factor that was equal to the ratio of the result of a CTDI simulation and an actual CTDI measurement with an ionization chamber, and multiplying by the ratio of the mAs value of the actual scan and that of the normalization (CTDI) scan.

During the CT scans, about one thousand projections were acquired per rotation. In order to keep simulation time manageable, only 60 equally-spaced projections were simulated per rotation with ~10,000,000 photons generated per projection. This number of photons guaranteed that the random error in the MC result was much smaller than the random error in a MOSFET measurement. This was checked by running the same simulation multiple times with different seeds for the random number generator. The X-ray tube start angle of the simulated scan was matched to the start angle of the actual scan, which was given by one of the DICOM tags, as were the number of rotations and the pitch.

Voxelized phantoms (voxel size = 3.9 × 3.9 × 4.1 mm^3 for adult phantoms; 2.3 × 2.3 × 2.0 mm^3 for infant phantom) were generated from reconstructed CT images by assigning materials and densities based on the Hounsfield Unit (HU) value of a voxel. Each voxel was designated as air (-1000 to -930 HU), lung (-930 to -200 HU), adipose tissue (-200 to -5 HU), water (-5 to 5 HU), soft tissue (+5 to +40 HU), skeletal muscle (+40 to + 400 HU), or cortical bone (> +400 HU) [22]. The material in the voxels at each MOSFET location was replaced with SiO_2 at a density such that the HU value was the same as in the scanned volume. The interaction of X-ray photons with the voxelized phantom was governed by

properties of the material within each voxel provided by the National Institute of Standards and Technology (NIST) database[23].

C. Dependence of c on measurement value

In order to verify that c is independent of MOSFET voltage we divided the measurements by MOSFET voltage into ten groups of about equal size and determined c for each group. Figures C1 and C2 show the estimate of c with 95% confidence interval, for each group, as a function of the average value of $\tilde{V}_j$ for that group, for 100 and 120 kVp, respectively. The graphs do not show a $\langle \tilde{V}_j \rangle$-dependent deviation that could be a strong indication of non-constancy of c.

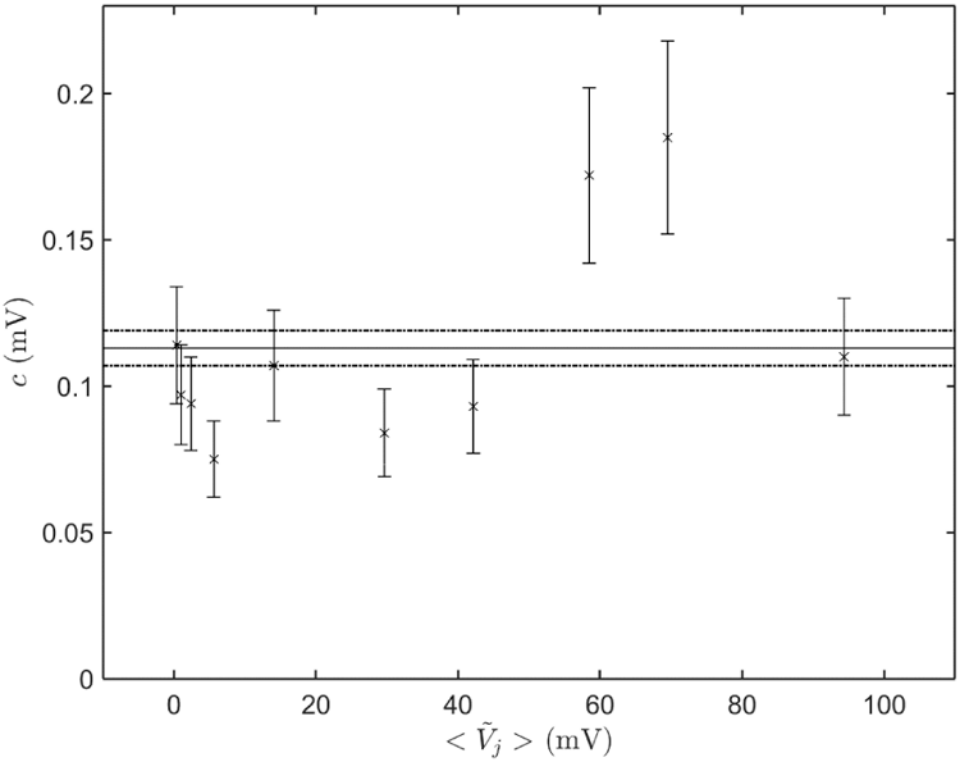

Figure C1.
Values of c with 95% confidence intervals obtained by grouping MOSFET voltage measurements at 100 kVp by value. The horizontal axis reports the average value of $\tilde{V}_j$ for each group. The horizontal lines denote the result obtained by using all measurements: c = 0.113±0.006 mV.

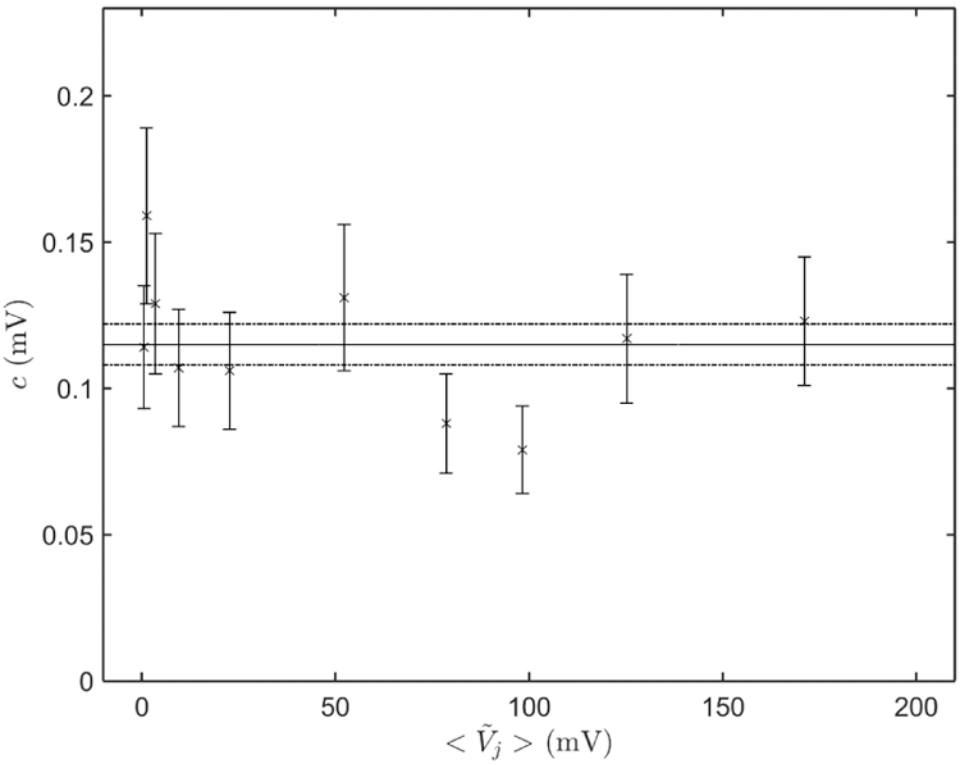

Figure C2.
Values of c with 95% confidence intervals obtained by grouping MOSFET voltage measurements at 120 kVp by value. The horizontal axis reports the average value of $\tilde{V}_j$ for each group. The horizontal lines denote the result obtained by using all measurements: c = 0.115mV±0.007 mv.

A typical value for the calibration factor of the MOSFETs that we used is 3 mV/mGy. Since the active volume of a MOSFET is about 0.2 mm × 0.2 mm × 1 μm[24] the energy deposition in that volume (containing SiO_2) is about 2.2×10^2 keV/mV. The average energy of a photon for a typical 120 kVp CT spectrum is about 65 keV in the in-beam region and the spectrum-averaged value of the ratio of the absorption coefficient and the attenuation coefficient[22], μ_{en}/μ, is 0.35, implying that for the photons that interact in a volume, 35% of the energy is deposited locally (the rest leaves the volume as scattered photons). In other words, there is 6.3×10^2 keV/mV of energy in the interacting photons, which corresponds to 9.7 (65 keV) photons/mV. Assuming Poisson statistics leads to a value for c of 1/(9.7/mV) = 0.10 mV. A similar calculation for 80 kVp and 100 kVp leads to essentially the same value (the increased absorption is almost exactly compensated by the lower average energy per photon).

References

1. Hurwitz LM, Yoshizumi TT, Goodman PC, Frush DP. Effective dose determination using an anthropomorphic phantom and metal oxide semiconductor field effect transistor technology for clinical adult body multidetector array computed tomography protocols. J Comput Assist Tomogr. 2007; 31(4):544–549. [PubMed: 17882029]

2. Peet DJ, Pryor MD. Evaluation of a MOSFET radiation sensor for the measurement of entrance surface dose in diagnostic radiology. Br J Radiol. 1999; 72(858):562–568. [PubMed: 10560338]
3. Ehringfeld C, Schmid S, Poljanc K, Kirisits C, Aiginger H, Georg D. Application of commercial MOSFET detectors for in vivo dosimetry in the therapeutic x-ray range from 80 kV to 250 kV. Phys Med Biol. 2005; 50(2):289–303. [PubMed: 15742945]
4. Brady SL, Kaufman RA. Establishing a standard calibration methodology for MOSFET detectors in computed tomography dosimetry. Med Phys. 2012; 39(6):3031–3040. [PubMed: 22755688]
5. Syam Kumar SA, Sukumar P, Sriram P, Rajasekaran D, Aketi S, Vivekanandan N. A patient-specific quality assurance study on absolute dose verification using ionization chambers of different volumes in RapidArc treatments. Med Dosim. 2012; 37(4):436–441. [PubMed: 22626968]
6. Bank MI. Ion chamber measurements of transverse gamma knife beam profiles. J Appl Clin Med Phys. 2002; 3(1):12–18. [PubMed: 11818000]
7. Yoshizumi TT, Goodman PC, Frush DP, Nguyen G, Toncheva G, Sarder M, Barnes L. Validation of metal oxide semiconductor field effect transistor technology for organ dose assessment during CT: comparison with thermoluminescent dosimetry. Am J Roentgenol. 2007; 188(5):1332–1336. [PubMed: 17449779]
8. Hurwitz LM, Yoshizumi TT, Reiman RE, Paulson EK, Frush DP, Nguyen GT, Toncheva GI, Goodman PC. Radiation dose to the female breast from 16-MDCT body protocols. Am J Roentgenol. 2006; 186(6):1718–1722. [PubMed: 16714665]
9. Nikolic B, Khosa F, Lin PJP, Khan AN, Sarwar S, Yam CS, Court LE, Raptopoulos V, Clouse ME. Absorbed Radiation Dose in Radiosensitive Organs During Coronary CT Angiography Using 320-MDCT: Effect of Maximum Tube Voltage and Heart Rate Variations. Am J Roentgenol. 2010; 195(6):1347–1354. [PubMed: 21098194]
10. Hurwitz LM, Reiman RE, Yoshizumi TT, Goodman PC, Toncheva G, Nguyen G, Lowry C. Radiation dose from contemporary cardiothoracic multidetector CT protocols with an anthropomorphic female phantom: implications for cancer induction. Radiology. 2007; 245(3): 742–750. [PubMed: 17923509]
11. Huggett J, Mukonoweshuro W, Loader R. A phantom-based evaluation of three commercially available patient organ shields for computed tomography X-ray examinations in diagnostic radiology. Radiat Prot Dosimetry. 2013; 155(2):161–168. [PubMed: 23222552]
12. Loader RJ, Gosling O, Roobottom C, Morgan-Hughes G, Rowles N. Practical dosimetry methods for the determination of effective skin and breast dose for a modern CT system, incorporating partial irradiation and prospective cardiac gating. Br J Radiol. 2012; 85(1011):237–248. [PubMed: 21896660]
13. AAPM. The measurement, reporting, and management of radiation dose in CT. AAPM Report No 96. 2008
14. Bauhs JA, Vrieze TJ, Primak AN, Bruesewitz MR, McCollough CH. CT dosimetry: comparison of measurement techniques and devices. Radiographics. 2008; 28(1):245–253. [PubMed: 18203941]
15. http://www.radcal.com/pdf/ew-10x5-chamber-spec-11-2-6.pdf
16. http://www.mosfet.ca/global/pdf/manuals/mobilemosfet.pdf
17. Whiting, BR. Medical Imaging: Physics of Medical Imaging. San Diego, CA: 2002. presented at the Proceedings of SPIE 4682. unpublished
18. Radcal Corporation. 426 West Duarte Road, Monrovia, California 91016, USA: http://www.radcal.com/10x6-3ct
19. Hintenlang D. TH-C-301-03: Utilization of MOSFET Dosimeters for Clinical Measurements in Radiology. Med Phys. 2011; 38:3861.
20. Koivisto JH, Wolff JE, Kiljunen T, Schulze D, Kortesniemi M. Characterization of MOSFET dosimeters for low-dose measurements in maxillofacial anthropomorphic phantoms. J Appl Clin Med Phys. 2015; 16(4):266–278. [PubMed: 26219008]
21. Best Medical Canada, Ltd. 413 March Road Ottawa, Ontario K2K 0E4, Canada: http://www.mosfet.ca/global/pdf/technotes/T7_101684_04_MOSFETspecs.pdf
22. ICRU. Tissue Substitutes in Radiation Dosimetry and Measurement. Bethesda, MD: International Commission on Radiation Units and Measurements; 1989.
23. National Institute of Standards and Technology. http://www.nist.gov/pml/data/xraycoef/index.cfm

24. Wang B, Kim CH, Xua XG. Monte Carlo modeling of a high-sensitivity MOSFET dosimeter for low- and medium-energy photon sources. Med Phys. 2004; 31(5):1003–1008. [PubMed: 15191284]

25. Report of AAPM Task Group 111. Comprehensive Methodology for the Evaluation of Radiation Dose in X-Ray Computed Tomography. American Association of Physicists in Medicine; Alexandria, VA: 2010.

26. Dixon RL, Boone JM. Analytical equations for CT dose profiles derived using a scatter kernel of Monte Carlo parentage with broad applicability to CT dosimetry problems. Med Phys. 2011; 38(7):4261–4264.

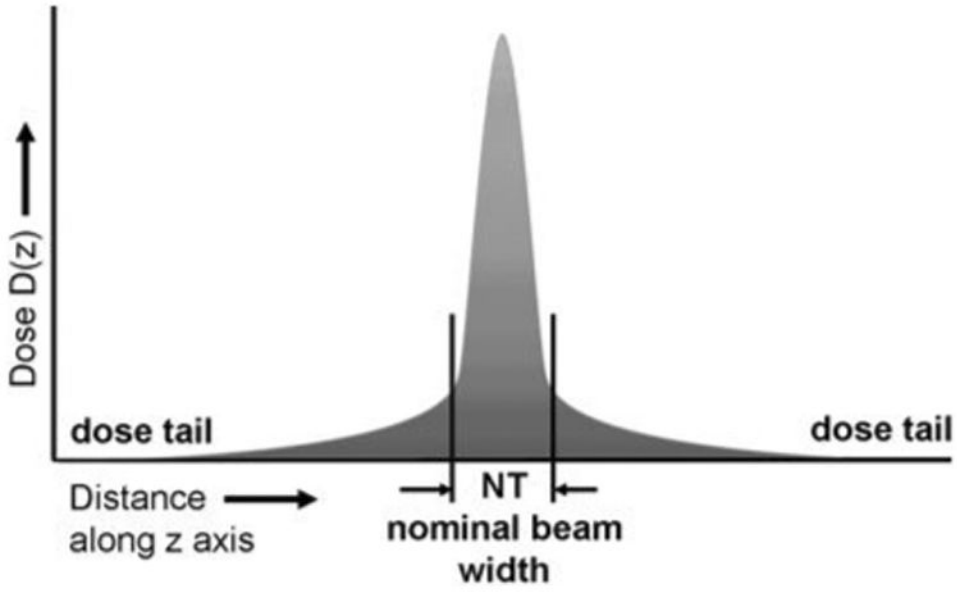

Figure 1.
Illustration of the axial scan radiation dose profile $D(z)$[14]

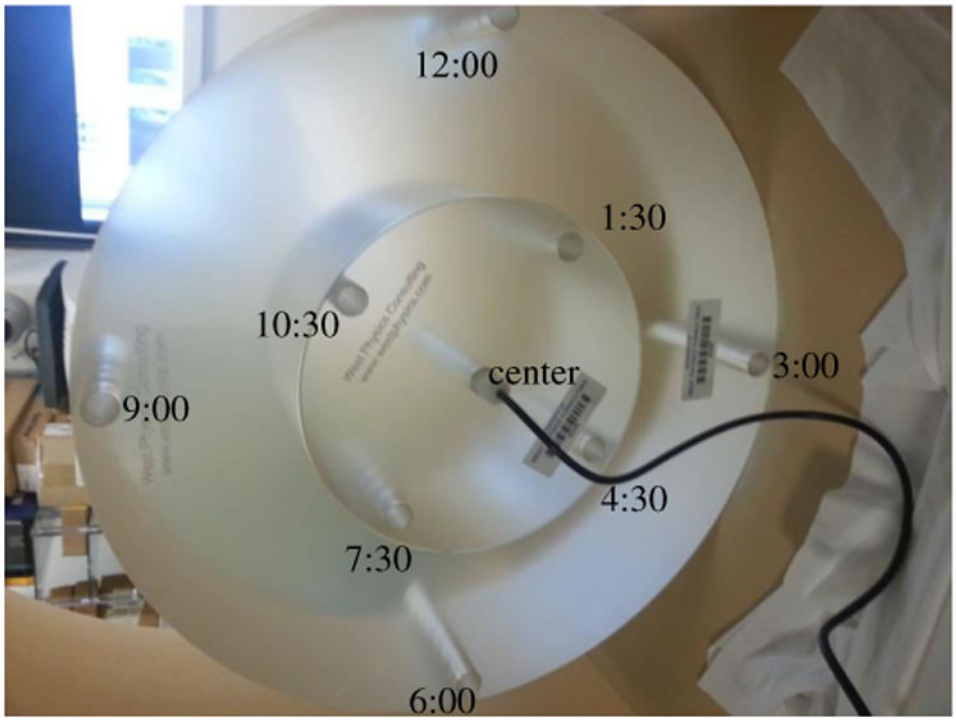

Figure 2.
CTDI phantom with nine holes, one at the center, four at the periphery, noted as clock positions 3:00, 6:00, 9:00, and 12:00, and four at the midway part, at clock positions 1:30, 4:30, 7:30 and 10:30, between center and periphery.

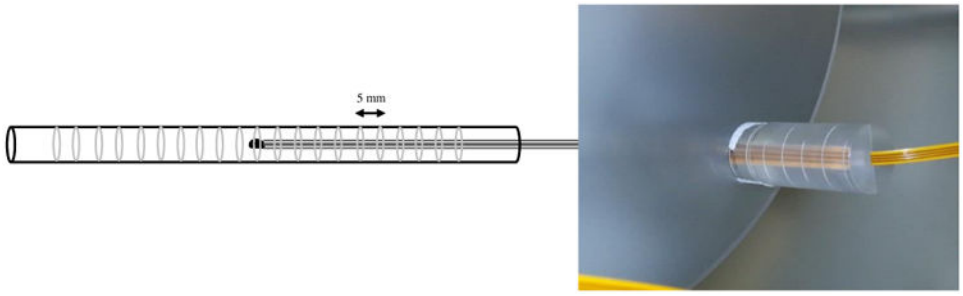

Figure 3.
Right image: A custom-made holder for a MOSFET, with lines at 5 mm intervals, that is used to move the MOSFET in discrete steps. Left image: A schematic depiction of the holder with the marked lines at 5 mm intervals containing a MOSFET centered on the z-axis.

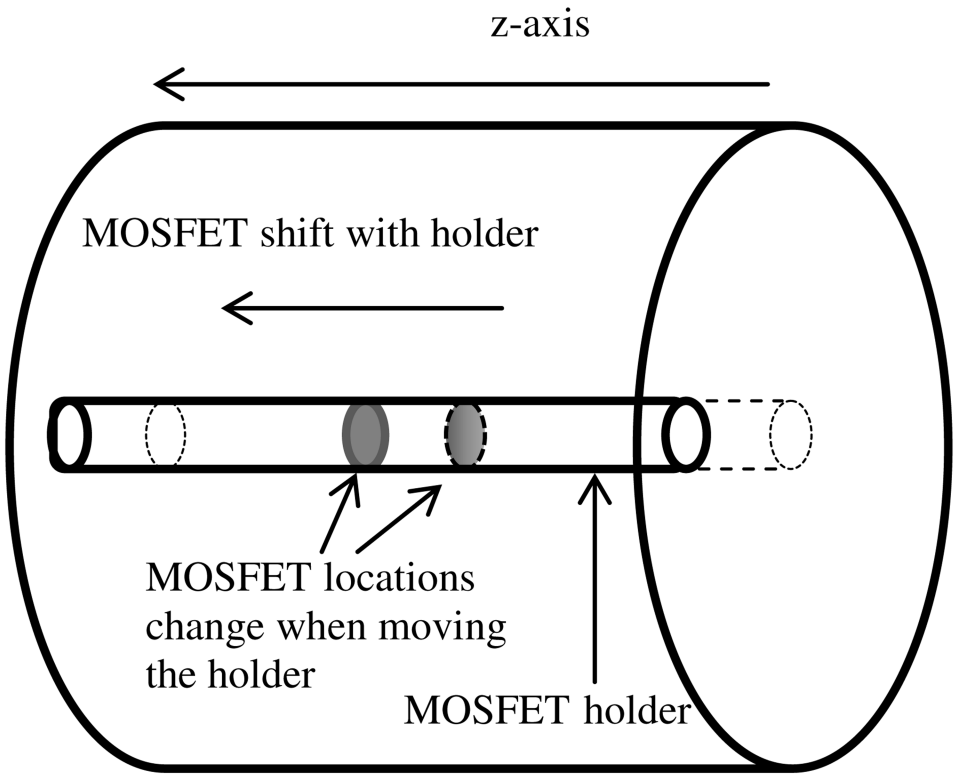

Figure 4.

Illustration showing the movement of the holder with MOSFET inside a single hole in z-direction in the CTDI phantom. In this illustration, holder and MOSFET had begun in the position denoted by the dashed lines and was moved to the left to the position denoted by the solid lines.

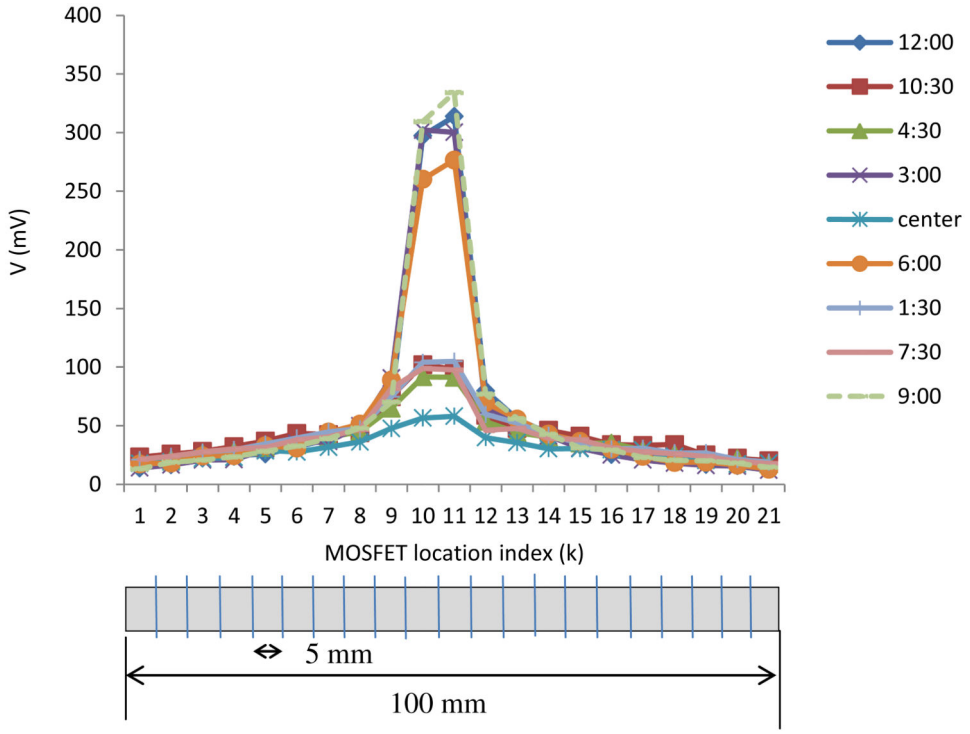

Figure 5.

MOSFET voltage V as a function of MOSFET location index $K = 1,\ldots, 21$, for the nine different holes in the CTDI phantom located at the specified clock positions, for a calibration measurement at 120 kVp. The locations are distributed over 100 mm with 5 mm separation.

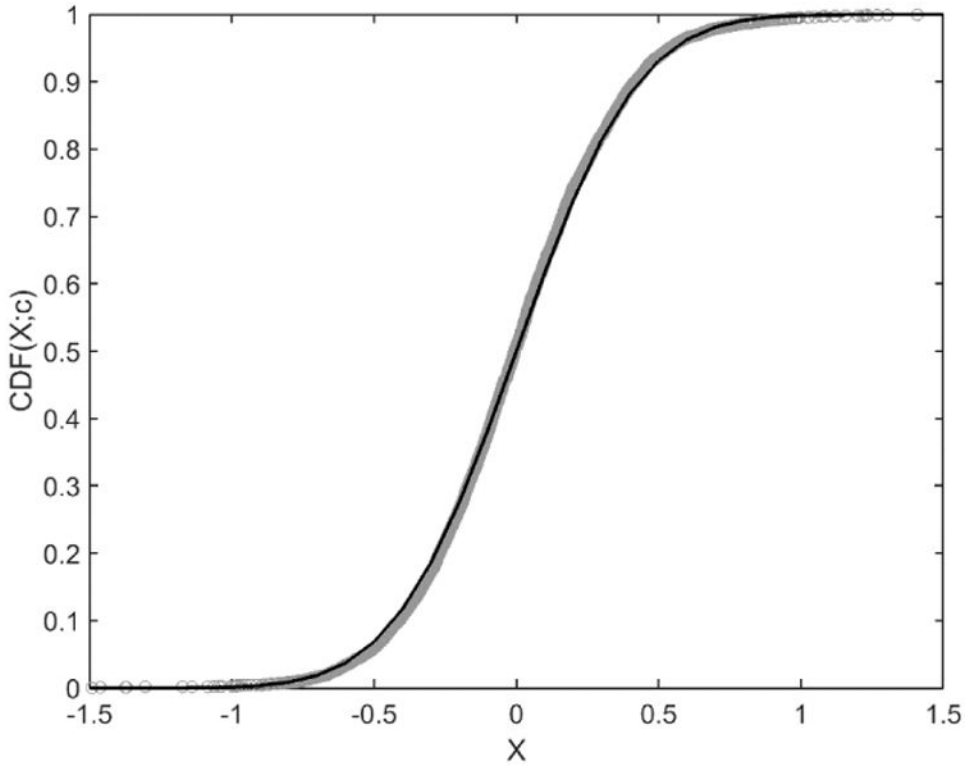

Figure 6.

Plot of the Cumulative Distribution Function (CDF) of the (start-angle corrected) data points (gray circles) and MLE fit (black solid line). Data is from all tube voltage measurements (80, 100,120 kVp).

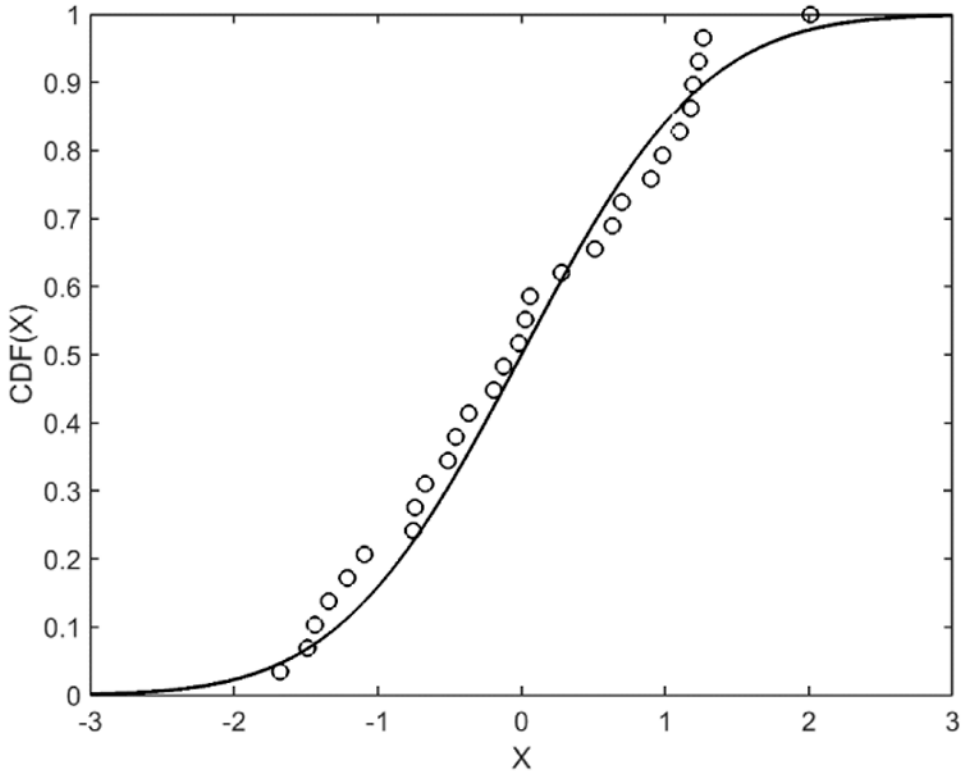

Figure 7.
Cumulative Distribution Function (CDF) of $\tilde{V}$ as a function of $X \equiv (\tilde{V} - \hat{\mu})/s$ (circles) and CDF of the standard normal distribution (solid line).

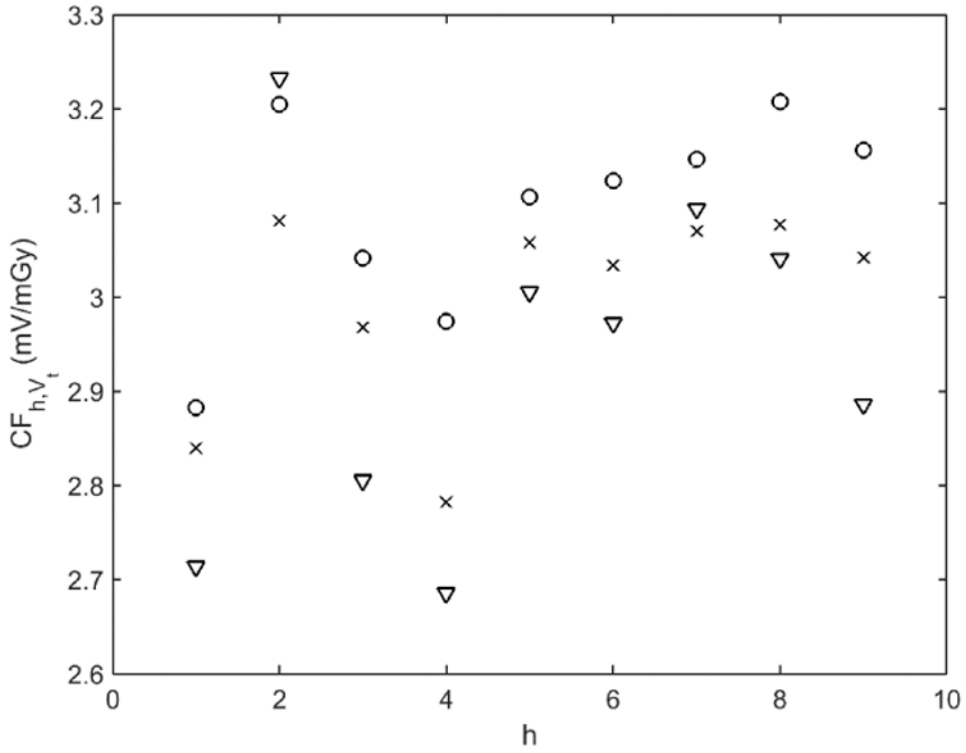

Figure 8.

Calibration factors, CF_{h,V_t}, for 80 kVp (circles), 100 kVp (crosses), and 120 kVp (triangles) for Site 1. The horizontal axis is the index of the CTDI hole (h): 1 = 3:00, 2=6:00, 3=9:00, 4=12:00, 5=1:30, 6=4:30, 7=7:30, 8=10:30, and 9=center.

Table 1

Calibration factors, CF_{V_t}, for tube voltages, V_t, of 80, 100, and 120 kVp, at two measurement sites: Site 1: Philips Healthcare, Cleveland, OH, and site 2: Cleveland Clinic, OH.

V_t (kVp)	CF_{V_t} [mV/mGy] Site 1	CF_{V_t} [mV/mGy] Site 2
80	3.03	3.13
100	2.94	2.99
120	2.88	2.87

Table 2

Calibration factors and CoVs for in-field and out-of-field calibrations, at different depths in the CTDI phantom.

	In-Field Calibration Factor [mV/mGy]	Out-of-field Calibration Factor [mV/mGy]	
Position	**MOSFET midway position**	**MOSFET in mid-position**	**Average of MOSFET in 3 positions, 1 cm apart**
12:00	2.91	3.13	3.42
3:00	2.83	3.28	3.19
6:00	2.91	2.86	2.89
center	2.91	3.09	3.25
Average	2.89	3.09	3.19
CoV [%]	1.4	5.56	6.91

CoV= coefficient of variation.